Korean J. Chem. Eng., 34(6), 1708-1720 (2017)
DOI: 10.1007/s11814-017-0056-7

pISSN: 0256-1115
eISSN: 1975-7220

Insight into adsorption mechanism of cationic dye onto agricultural residues-derived hydrochars: Negligible role of π-π interaction

Hai Nguyen Tran*,,†, Sheng-Jie You**,†, and Huan-Ping Chao**,†**

*Department of Civil Engineering, Chung Yuan Christian University, Chungli 320, Taiwan
**Department of Environmental Engineering, Chung Yuan Christian University, Chungli 320, Taiwan
(*Received 7 January 2017 • accepted 27 February 2017*)

Abstract−Hydrochars derived from golden shower pod (GSH), coconut shell (CCH), and orange peel (OPH) were synthesized and applied to remove methylene green (MG5). The results indicated that the hydrochars possessed low specific surface areas (6.65-14.7 m^2/g), but abundant oxygen functionalities (1.69-2.12 mmol/g). The hydrochars exhibited cellular and spherical morphologies. Adsorption was strongly dependent on the solution pH (2-10) and ionic strength (0-0.5 M NaCl). Equilibrium can be quickly established in the kinetic study (60-120 min). The maximum Langmuir adsorption capacities at 30 °C followed the order GSH (59.6 mg/g)>CCH (32.7 mg/g)>OPH (15.6 mg/g)> commercial glucose-prepared hydrochar (12.6 mg/g). The dye adsorption efficiency was determined by the concentrations of oxygen-containing functionalities on the hydrochar surface. The adsorption process occurred spontaneously ($-\Delta G^o$) and exothermically ($-\Delta H^o$). Desorption studies confirmed the reversible adsorption process. Oxygenation of the hydrochar surface through a hydrothermal process with acrylic acid contributed to increasing MG5 adsorption and identifying the negligible role of π-π interaction to the adsorption process. The analysis of Fourier transform infrared spectrometry demonstrated that the aromatic C=C peak did not significantly decrease in intensity or shift toward higher/lower wavenumbers after adsorption, which further confirms the insignificant contribution of π-π interaction. Electrostatic attraction played a major role in adsorption mechanisms, while minor contributions were accounted for hydrogen bonding and n-π interactions. The primary adsorption mechanisms of MG5 onto hydrochar were similar to biosorbent, but dissimilar to biochar and activated carbon (i.e., π-π interaction and pore filling).

Keywords: Hydrothermal Treatment, Hydrochar, Adsorption Mechanism, Cationic Dye, Oxygenation Method, π-π Interaction

INTRODUCTION

The presence of dyes and pigments in effluents is of enormous concern to public health around the world because of their toxic, carcinogenic, mutagenic, and allergic nature. In addition, the untreated discharge of a great volume of wastewater has attracted more attention because of aesthetically displeasing reasons and environmentally adverse problems, with potential health risks for humans. It is estimated approximately 200,000 tons of dye are discharged by the textile industry to the water environment [1], and approximately 10,000 tons of dye produced every year [2]. During the dyeing process, it is anticipated that the losses of colorants to the environment can reach 10-50% [1].

It might be difficult to decolor or treat dye-containing water and wastewater streams since dye molecules tend to have relatively strong recalcitrance and resistance to aerobic digestion as well as high stability to light, heat, and oxidizing agents [3]. Among the typical methods for removal dyes (i.e., membrane, biological treatment, and oxidation), adsorption can be considered the most economically favorable technology because of its relative high removal efficiency, high reversibility, and low operation costs [4].

Although raw lignocellulose biomasses derived from agricultural wastes can serve as the low-cost and renewable adsorbents for removal of dye from aqueous media because of active functional groups on their surface, there are several controversial problems when they were used directly for water treatment. This is because the water after being treated had a high level of chemical oxygen demand, biological chemical demand, and total organic carbon, which results from releases of soluble organic compounds (i.e., lignin, tannin, and pectin) during adsorption process [5]. These releases can cause the second pollution or make the treated water to be light yellow or brown colors.

Biochar, a state carbon-enriched and porous material, is produced through the pyrolysis process in an inert atmosphere (i.e., N_2 or Ar atmosphere), in a non-circulating air atmosphere (i.e., within lid-enclosed crucible), or even under vacuum condition at a high carbonization temperature [6,7]. This process is also known as a dry pyrolysis. Our recent research suggested that the cationic dye adsorption capacities of agricultural residues-developed biochars were limited and the adsorption process was irreversible. The primary adsorption mechanisms were regarded as π-π interaction and non-micropore filling (un-published data). Analogous adsorption mechanisms were also observed for the adsorption of cationic dye (i.e., MG5) onto other carbonaceous porous materials, such as commercial activated carbon [8] and synthesized activated car-

†To whom correspondence should be addressed.
E-mail: trannguyenhai2512@gmail.com, sjyou@cycu.edu.tw, hpchao@cycu.edu.tw

bons [9].

Recently, the hydrothermal carbonization (HTC)—a thermochemical conversion technique that uses subcritical water for the conversion of wet or dry biomass to carbonaceous products (also known as hydrochar) through fractionation of the feedstock—has attracted more attention. This process can produce carbonaceous materials with a high density of oxygenated functional groups due to the decrease of pH during hydrothermal carbonization of biomass [10-12]. Furthermore, the hydrothermal carbonization (wet carbonization) is more economically efficient than pyrolysis process (dry carbonization), because it requires lower carbonization temperature and does not require energies for desiccation of biomass.

Like biochar and activated carbon, hydrochar also possesses the aromaticity of carbon structures that results from hydrothermal carbonization of carbohydrates in (hemi-) cellulose compounds [13]. Generally, the H/C molar ratio can be used as an indicator of the degree of aromatization and carbonization. Hydrochar generally has higher H/C and O/C ratios similar to natural coal than the solids (i.e., biochar) resulting from dry pyrolysis [10,12]. In addition, although chars (i.e., hydrochar, biochar, and activated carbon) contain extensive aromatic structures, they are arranged differently. For example, the structure of biochar comprises turbostratically arranged sheets of conjugated aromatic carbon, while carbon sphere (i.e., glucose-derived hydrochar) is hypothesized to exhibit an aromatic core of cross-linked furanic rings with mainly aldehydic and carboxy functional end groups [10].

The presence of the aromatic C=C bonds in hydrochar might be expected to form π-π interactions between the π-electrons of hydrochar and the π-electrons of the aromatic rings of an adsorbate (i.e., dye or phenol). Our previous studies [8,9] proved that the oxygenation process of the surface of carbonaceous materials (i.e., biochar and activated carbon) through a hydrothermal process with acrylic acid can enhance the density of oxygen-containing groups on their surface without significantly affecting their textural properties (i.e., specific surface area and total pore volume). Oxygenation of the surface of carbonaceous materials resulted in a dramatic decrease in MG5 adsorption, which supported the hypothesis that π-π interactions play a primary role in MG5 adsorption.

In this study, we prepared hydrochars derived from three agricultural wastes (golden shower pod, coconut shell, and orange peel) through a hydrothermal carbonization process. These hydrochars were characterized by Brunauer-Emmett-Teller (BET) surface area, scanning electron microscopy, Fourier transform infrared spectroscopy, point of zero charge, and Boehm titration. The hydrochar samples were directly used without any treatments for the experiments of removal of a cationic methylene green 5 (MG5). The adsorption processes were conducted in batch experiments under various operating conditions, such as various pH values of initial dye solutions, NaCl concentrations, contact times, MG5 initial concentrations, solution temperatures, and desorption agents. Besides non-oxygenated-hydrochars, oxygenated-hydrochar samples were also prepared through a hydrothermal process with acrylic acid. A pure hydrochar sample derived from the commercial *D*-glucose was additionally prepared for comparison. The contributions of π-π interactions were investigated by comparison of (1) the FTIR results before and after adsorption, and (2) the adsorption results between non-oxygenated and oxygenated-hydrochars.

MATERIALS AND METHODS

1. Sample Preparation

1-1. Feedstock Preparation

The biomasses of golden shower pod, coconut shell, and orange peel, were collected from a local market in Taiwan. They were washed with tap water and then with deionized distilled water to remove any water-soluble impurity and adhering dirt. After that, they were dried at 80 °C for 48 h to remove excess water content. The dried biomasses were sieved into particles ranging from 0.106 to 0.25 mm and used as carbohydrate precursors for the preparation of hydrochar.

1-2. Hydrochar Preparation

Approximately 20 g the precursor was mixed with 120 mL of deionized distilled water in 200 mL Teflon-lined autoclave. After 24 h hydrothermal carbonization (HTC) at 190 °C, the brown precipitate (hydrochar) was separated using filtration and washed repeatedly with HCl 0.1 M, followed by washing with deionized distilled water until the filtrate reached a constant value. The hydrochar samples were collected, sieved, and dried at 105 °C for 24 h to remove excess water and moisture. The samples were stored in airtight bottles and used as potential adsorbents without any further treatments [12]. For convenience, the hydrochar samples were labeled according to their precursors, such as golden shower pod (GSH), coconut shell (CCH), and orange peel (OPH) hydrochars. Furthermore, the hydrochar derived from the commercial *D*-glucose (GH) was prepared under the same aforementioned synthesis procedure for the comparisons on maximum adsorption capacity and morphology [14].

We also investigated the effects of (1) the times of hydrothermal carbonization process, and (2) the presence of NaOH on the formation of carbon spheres in the hydrochar samples. The results were evaluated by morphological analysis using scanning electron microscopy.

2. Hydrochar Properties

Textural properties were measured using nitrogen adsorption–desorption isotherms (Micromeritics ASAP 112 2020 sorptometer) at 77 K. Meanwhile, the morphology of the hydrochars was obtained using scanning electron microscopy (SEM; Hitachi S-4800, Japan).

Surface chemistry of the hydrochar was identified by three techniques. First, the functional groups present on the hydrochar's surface were detected using Fourier transform infrared spectroscopy (FTIR; FT/IR-6600 JASCO); the hydrochar particles were pelleted mixing with pure KBr. Secondly, the pH value of the hydrochar at the point of zero charge (pH_{PZC}) was determined using the common "drift method" [6]. Recently, we [8] investigated the effects of operation conditions on the pH_{PZC} of commercial activated-charcoal. The results demonstrated that the point of zero charge (9.81± 0.07) of charcoal was insignificantly dependent on the operation conditions (i.e., CO_2, solid/liquid ratio, electrolyte type, electrolyte concentration, and contact time). Thirdly, the amount of acidic groups and basic sites on the hydrochar's surface was determined

through Boehm titration by following the standardization protocol proposed by Goertzen and coworkers [15]. The numbers of moles of adsorbent surface functionalities were calculated using the equations reported in our recent work [12].

3. Adsorption Study

3-1. Batch Adsorption Experiments

The effect of pH of the initial dye solutions (2.0-10±0.2) was conducted at 30 °C by mixing 25 mL solution containing approximately 300 mg/L of MG5 with 0.1 g of the hydrochar. Similarly, the effect of ionic strength was measured in various NaCl concentrations (0 M-0.5 M). Meanwhile, the adsorption kinetics was investigated for a series of 150-mL Erlenmeyer flasks containing 50 mL of MG5 (~300 mg/; 7.0±0.2) at 30 °C and 0.2 g of the hydrochar. The adsorption isotherms were carried out with various initial MG5 concentrations (100-1,100 mg/L; pH 7.0) at different experimental temperatures (30, 40, and 50 °C). The dye-hydrochar mixture was shaken using an orbital shaking incubator (S300R-Firstek) at 150 rpm. After desirable time intervals, the mixture was speared using glass fiber filters. The MG5-loaded hydrochar was rinsed with deionized distilled water, dried, and stored for the further experiment (i.e., FTIR and desorption). The MG5 concentration in solution was determined using ultraviolet-visible spectrophotometry (Genesys 10 UV-Vis; Thermo Scientific) at maximum wavelengths (Fig. 1). The amount of MG5 uptake at equilibrium, q_e (mg/g), was calculated by the mass balance equation:

$$q_e = \frac{(C_o - C_e)}{m_1} V_1 \quad (1)$$

where C_o (mg/L) and C_e (mg/L) is the MG5 concentrations at beginning and equilibrium, respectively; m_1 (g) is the mass of used hydrochar; and V_1 (L) is the volume of the MG5 solution. All batch adsorption experiments were at a constant solid/liquid ratio of approximately 4.0 g/L.

Adsorption reversibility was determined by desorption experiments using the following solvents as desorbing agents: deionized water pH 2, HCl (0.1 M), methanol, and NaCl (0.1 M). A given mass of MG5-laden hydrochar (m_2) was desorbed by using 0.025 L of various desorbing agents (V_2). The amount of MG5 remaining on the hydrochar was estimated by the following mass-balance relationship:

$$q_r = q_e - q_d = q_e - \frac{C_d}{m_2} V_2 \quad (2)$$

where q_r (mg/g) is the mass of MG5 that remained adsorbed at the end of desorption study, C_d (mg/L) is the concentration of MG5 in the solution after desorption; and q_d (mg/g) is the mass of MG5 desorbed if the adsorption was reversible.

An additional experiment was conducted to identify the presence of any π-π interactions. Approximately 5.0 g of the hydrochar was immersed with 100 mL deionized distilled water containing of acrylic acid (i.e., 20 mL, 30 mL, or 50 mL). The mixture was stirred at 300 rpm for 1 h and subsequently transferred into 200 mL Teflon-lined autoclave. After a 24-h hydrothermal process at 190 °C formed oxygenated-hydrochar, a brown solid, which was then separated from solution and washed with deionized distilled water until the pH of filtrate reached a constant value [8,9].

3-2. Statistical Analysis

All experiments were conducted in triplicate, and the results are expressed as a mean±standard deviation. Trial-and-error nonlinear methods were performed using the Solver add-in, Microsoft Excel, to compute parameters of the isotherm and kinetic models. To identify the best-fit model for the adsorption process, calculation of the chi-squared (χ^2, Eq. (3)) value is recommended in addition to calculations of the coefficient of determination (R^2, Eq. (4)) for the nonlinear method [6,9]. The statistics of the chi-square test is basically the sum of the squares of the differences between experimental data and data obtained through calculations by using the models, and each squared difference is then divided by the corresponding data obtained through calculations by using the models.

$$\chi^2 = \sum \frac{(q_{e,exp} - q_{e,cal})^2}{q_{e,cal}} \quad (3)$$

$$R^2 = 1 - \frac{\sum (q_{e,exp} - q_{e,cal})^2}{\sum (q_{e,exp} - q_{e,mean})^2} = \frac{\sum (q_{e,cal} - q_{e,mean})^2}{\sum (q_{e,cal} - q_{e,mean})^2 + \sum (q_{e,cal} - q_{e,exp})^2} \quad (4)$$

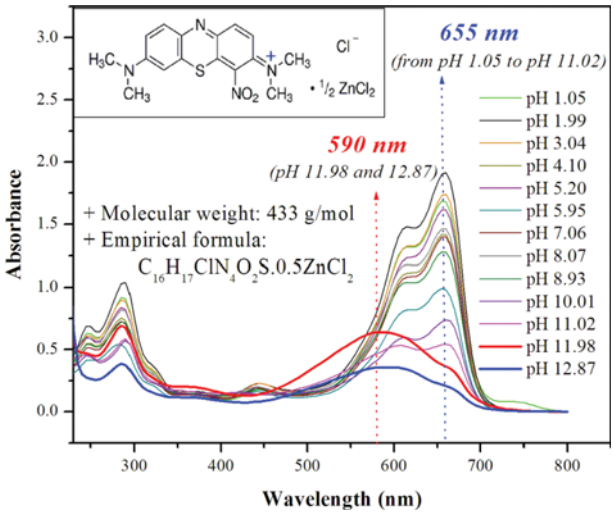

Fig. 1. Effect of pH of the MG5 solution on λ_{max} values (without adsorbent) (data published in our previous paper [9]).

Table 1. Some basic properties of the synthesized hydrochar samples

	Unit	GSH	CCH	OPH	GH
1. Textual properties					
BET surface area	m^2/g	14.7	6.65	6.99	7.08
Langmuir surface area	m^2/g	37.7	17.4	15.1	9.79
Total pore volume ($\times 10^{-3}$)	cm^3/g	76.2	2.62	2.49	8.25
2. Surface chemistry					
Total acidic groups	mmol/g	2.12	1.96	1.69	-
+Phenolic	mmol/g	0.53	0.47	0.34	-
+Lactonic	mmol/g	0.83	0.85	0.94	-
+Carboxylic	mmol/g	0.76	0.67	0.41	-
Total basic groups	mmol/g	0.10	0.34	0.86	-
pH_{PZC}	-	4.30	5.53	6.58	-

where $q_{e,exp}$ (mg/g) is the amount of MG5 uptake at equilibrium obtained from Eq. (1), $q_{e,cal}$ (mg/g) is the amount of MG5 uptake achieved from the model after using the Solver add-in, and $q_{e,mean}$ (mg/g) is the mean of $q_{e,exp}$ values.

The effects of temperatures on the maximum adsorption capacity of MG5 (Q^{o}_{max}) onto the hydrochar were statistically analyzed by using Statgraphics Plus 3.0 statistical program. Differences were considered significant at $p<0.05$ [6].

All chemicals used in this study were of analytical reagents grade.

RESULTS AND DISCUSSION

1. Hydrochar Characterization

A series of experiments were conducted to explore the formation of carbon spheres from the agricultural wastes. The experiments comprised the effects of HTC times (12 h, 24 h, and 72 h) and NaOH (0 M, 0.05 M, 0.1 M, 0.2 M, 0.5 M, and 1 M) on the spherical density of agricultural wastes-derived hydrochars. Surprisingly, most of the experimental performances demonstrated that

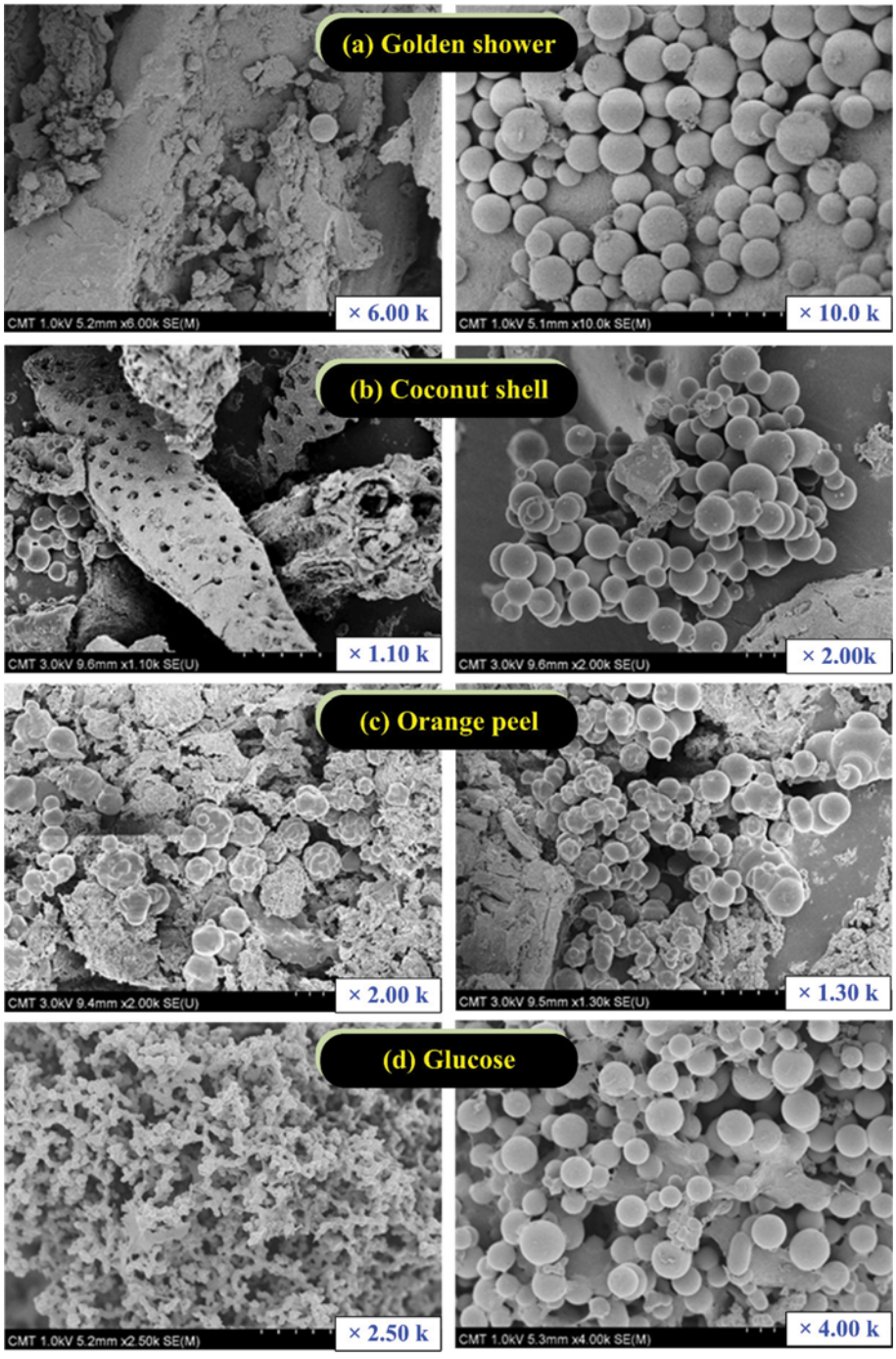

Fig. 2. SEM images of the hydrochar samples prepared from (a)-(c) agricultural wastes and (d) commercial glucose (Experimental conditions: 190 °C, 24 h, and 0 M NaOH).

there were no spherical morphologies observed by SEM (data not shown), except for the sample examined at the HTC condition of 24 h and 0 M NaOH. Therefore, the hydrothermal process of the agricultural wastes and commercial glucose was carried out at 190 °C for 24 h in an autoclave containing 120 ml of deionized distilled water.

The textural properties of the synthesized hydrochars are listed in Table 1. Obviously, the hydrochars possess hardly any porosity (i.e., low BET specific surface area and limited pore volume), which accords with their poor and heterogeneous morphology observed in Figs. 2(a)-(c). Similarly, the commercial glucose-derived carbon sphere (GH) also exhibits low specific surface area and total pore volume. Therefore, the adsorption affinity of these hydrochars toward MG5 molecules was expected through the functional oxygen-containing groups (i.e., -COOH and -OH) on their surfaces.

A scanning electron micrograph of the commercial glucose-derived carbon sphere is presented in Fig. 2(d). As expected, GH exhibits interconnected spheres with relatively uniform sizes, smooth outer surfaces, regular spherical shapes, and high purity [14]. According to Sevilla and Fuertes [16], the formation of the carbon-rich solid through the hydrothermal carbonization of glucose is attributed to dehydration, condensation, or polymerization and aromatization reactions. Essentially, every hydrochar particle (carbon-rich solid) often consists of two parts: hydrophobic core (a highly aromatic nucleus) and hydrophilic shell (outer layer; a high concentration of reactive oxygen functional groups like hydroxyl/phenolic, carbonyl, or carboxylic) [17].

The morphologies of agricultural wastes-derived carbon spheres (i.e., GSH, CCH, and OPH) are displayed in Figs. 2(a)-(c) (right-hand side). Clearly, these hydrochar samples also exhibit micrometer-sized spheres. The density limitation of sphere-like microparticles resulted from the presence of high lignin content in the lignocellulose materials [12]. Lignin compound with its greater chemical stability can be only partially degraded during HTC. Correspondingly, the original skeleton of the particles is mainly preserved [18], and the particles retain the cellular appearance of the raw materials [19]. Our previous study [12] showed that the hydrothermal process at 190 °C can completely decompose the hemicellulose component of raw GS, which was endorsed by the disappearance of the peak corresponding to the decomposition of hemicellulose in the thermogravimetric curve. In contrast, the cellulose and lignin in GS might be partly decomposed during HTC.

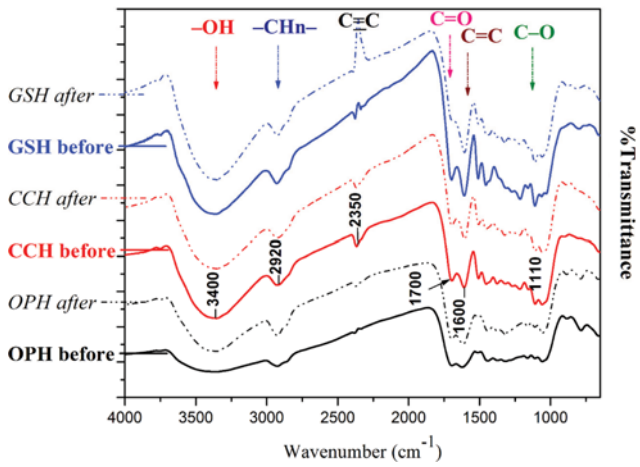

Fig. 3. FTIR spectra of the hydrochar samples before and after adsorption of MG5 (without baseline correction).

The qualitative information on the functional groups on the surface of hydrochar is depicted in Fig. 3. The sharp bands observed at approximately 3,400 cm^{-1} belong to the (O-H) stretching vibrations in the hydroxyl group of phenolic or carboxylic groups. Similarly, the moderate peaks at around 2,920 cm^{-1} are characteristic of either asymmetric or symmetric C-H stretching vibrations of the methyl (-CH_3-) and methylene (-CH_2-) groups. Moreover, the characteristics of carboxylic and lactonic groups (C=O) are endorsed by the well-defined peaks at approximately 1,700 cm^{-1}. Meanwhile, the C=C double bonds in aromatic rings are evident from the bands at around 1,600 cm^{-1}. Lastly, the infrared peaks at approximately 1,100 cm^{-1} are related to stretching C-O groups.

Oxygen-carrying functional groups on the hydrochar's surface can be classified into acidic and basic groups. The quantitative information on the superficial acidic and basic groups, which were determined by Boehm titration, is provided in Table 1. Therefore, it can be concluded that the hydrochar possesses a high concentration of reactive oxygen functionalities on their surface.

The electrical state of the hydrochar's surface in a solution is characterized by the point of zero charge (PZC). The PZC is defined as the pH value at which the net surface charge (external and internal) is zero. As shown in Fig. 4(a), the pH_{PZC} values of the hydrochar samples followed the order: OPH (6.58)>CCH (5.53)>GSH (4.30). Higher PZC values often coincide with a lower density of acidic groups on the surface: OPH (1.69 mmol/g)<CCH (1.96 mmol/g)<GSH (2.12 mmol/g).

2. Effect of pH and Ionic Strength

The effects of pH of the initial MG5 solution and the presence of the electrolyte in the MG5 solution on the adsorption ability of hydrochars are given in Figs. 4(b) and 4(c), respectively.

Obviously, the amount of adsorbed dye was strongly dependent on the tested solutions pH. The adsorption amount increased when the solutions pH increased. The enhancement might be ascribed in the presence of electrostatic attraction between the carboxylate (-COO^-) ions on the hydrochar's surface and cationic MG5 molecules. The p*K*a value of carboxylic groups is approximately 4.0. When the solutions pH is higher this p*K*a value, the surface charge of the hydrochar will become predominantly negative because of the dissociation of carboxylic groups (-COOH). This conclusion is in a good agreement with the observation of solutions pH after adsorption (Fig. 4(d)). The phenomenon of dissociation and ionization can be endorsed by the decrease of pH values after adsorption when solutions pH higher 4.0 and near pH_{PZC}. Furthermore, when the solutions pH are higher 8.0, the amount of dye removal can additionally increase because of the dissociation of phenolic groups (p*K*a~8.0-9.0) on the hydrochar's surface.

Notably, the hydrochars samples were still able to adsorb MG5 molecules at a low pH level (~2.0) although the presence of excess H^+ ions at this level from the system has strong competition with the cationic MG5 molecules for the active adsorption sites. The result confirmed that the contributions of other mechanisms (nei-

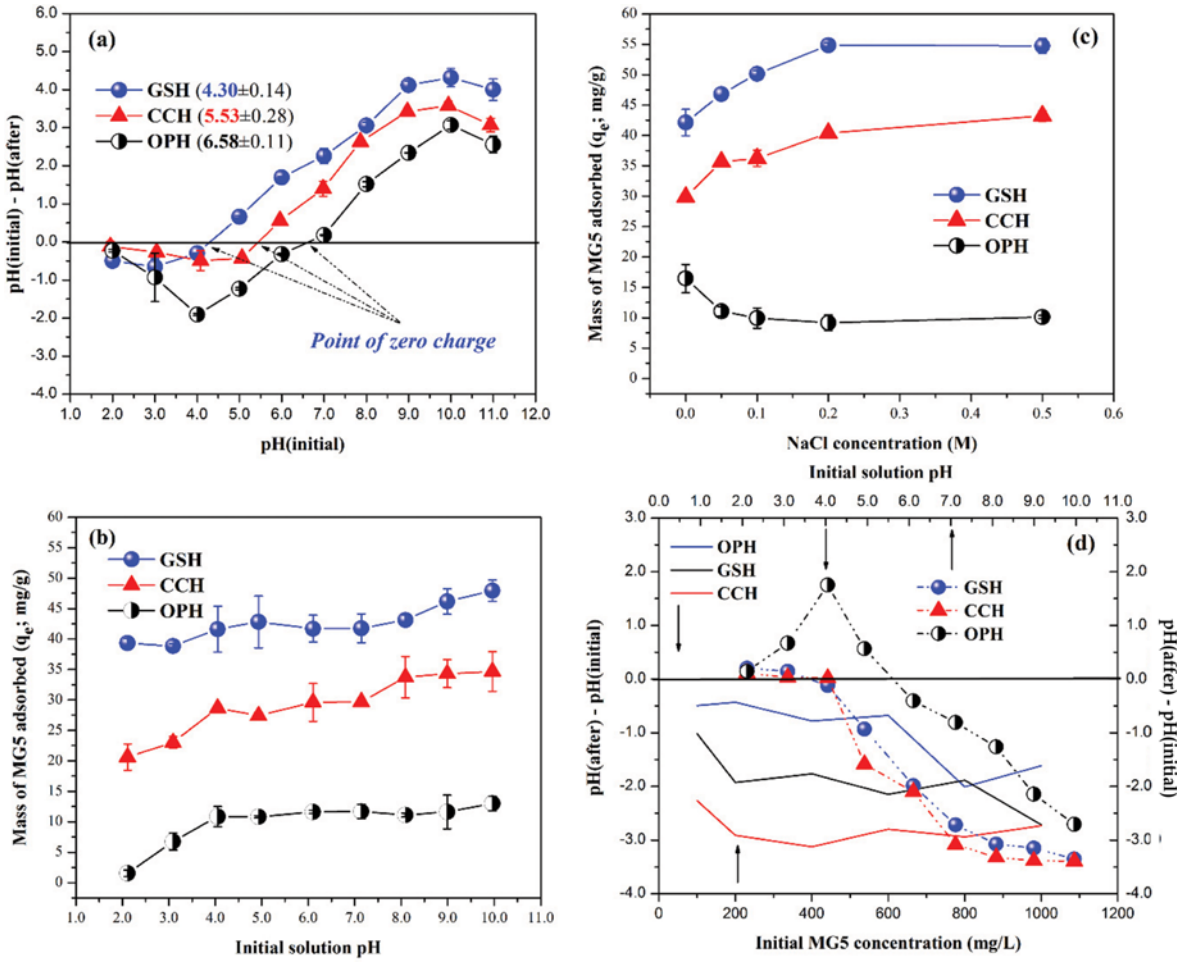

Fig. 4. (a) Point of zero charge of the hydrochar, (b) pH dependence on adsorption capacity, (c) effect of ionic strength on adsorption capacity, and (d) pH values after adsorption (Experimental conditions: (a) initial MG5 concentrations approximately 340 mg/L, contact time 24 h, temperature 30 °C, 0 M NaCl; and (c) initial MG5 concentrations approximately 340 mg/L, contact time 24 h, temperature 30 °C, pH 7.0).

ther hydrogen bonding nor n-π interactions) along with electrostatic attraction.

Similar to the pH dependence, the dye adsorption phenomenon was also affected by the presence of a univalent electrolyte in the solution. Fig. 4(c) indicates that the addition of the electrolyte ionic had both negative and positive effects on the dye removal process. The amount of dye adsorbed onto OPH decreased remarkably by 44% when the NaCl concentration increased from 0 M to 0.2 M; and with further increasing NaCl concentration, the amount of MG5 uptake decreased negligibly (Fig. 4(c)). This is because of (1) a screening effect (known as the electrostatic screening) between the positively charged OPH's surface and MG5 molecules, and (2) the competition phenomenon between Na^+ ions and MG5 cations for the adsorbing sites on the OPH's surface ($-COO^-$).

In contrast, the GSH and CCH samples demonstrated that their adsorption capacities toward MG5 were enhanced by the NaCl ions added to the dyebath (Fig. 4(c)). An analogous result was reported by Doğan and coworkers [20], who observed the biosorption of phenomenon methylene blue onto hazelnut shell. The enhancement was attributed to (1) an increase in the degree of

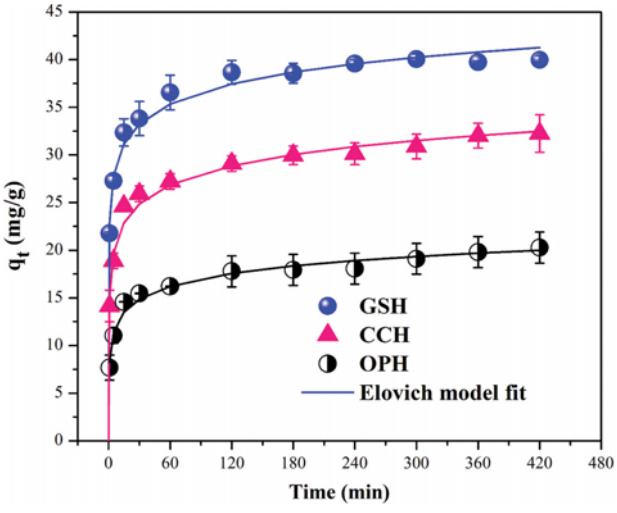

Fig. 5. Adsorption kinetics of MG5 adsorption onto three hydrochar samples (Experimental conditions: 0 M NaCl, temperature 30 °C, initial MG5 concentration 340 mg/L, and initial solution pH 7.0).

dissociation of the dye molecules by facilitating the protonation [20], and (2) partial neutralization of the positive charge on the hydrochar's surface and a consequent compression of the electrical double layer by the Cl^- anion [21].

3. Adsorption Kinetics

Fig. 5 presents the effects of contact time on the adsorption process of MG5. The amount of adsorbed dye increased consecutively during the initial 15 minutes of the contact interval; subsequently, the adsorption amount increased slightly until the equilibrium was established at approximately 60-120 min. Instantaneous adsorption phenomenon indicated that the hydrochar samples have a strong affinity toward the cationic dye molecules [9].

In this study, the adsorption mechanisms might be evaluated based on the pseudo-first-order, pseudo-second-order, and Elovich models. The non-linearized forms of the pseudo-first-order model [22], pseudo-second-order model [23], and Elovich model [24] are mathematically expressed in Eqs. (5), (6), and (7), respectively. Because the hydrochar was non-porous materials (low BET surface area and total pore volume), the intra-particle diffusion model might not be appropriate to apply in this study.

$$q_t = q_e(1 - e^{-k_1 t}) \tag{5}$$

$$q_t = \frac{q_e^2 k_2 t}{1 + k_2 q_e t} \tag{6}$$

$$q_t = \frac{1}{\beta}\ln(1 + \alpha\beta t) \tag{7}$$

where k_1 (1/min) and k_2 (g/mg×min) are the rate constants of the pseudo-first-order and pseudo-second-order models, respectively; α (mg/g×min) is the initial adsorption rate; β (mg/g) is the desorption constant during any one experiment; and q_e and q_t are the amounts of MG5 uptake per mass of the hydrochar at equilibrium and at any time t (min), respectively.

Table 2. Corresponding kinetic parameters for MG5 adsorption onto the hydrochar samples

	GSH	CCH	OPH
$q_{e,exp}$	39.66	30.93	17.93
Pseudo-first-order model			
$q_{e,cal}$	36.87	29.01	17.76
k_1	0.766	0.306	0.235
R^2	0.582	0.663	0.708
χ^2	4.305	8.099	5.874
Pseudo-second-order model			
$q_{e,cal}$	38.19	29.94	18.39
k_2	0.024	0.017	0.024
R^2	0.826	0.858	0.863
χ^2	2.154	2.699	1.752
Elovich model			
α	5,743	527.2	131.4
β	0.329	0.346	0.513
R^2	0.975	0.979	0.980
χ^2	0.271	0.304	0.212

Note: the units of kinetic parameters are q_e (mg/g), k_1 (1/min), k_2 (g/mg×min), α (mg/g×min), and β (mg/g)

The calculation results of kinetic adsorption parameters from the models are given in Table 2. According to the analysis of non-linear determination coefficients (R^2) and chi-square statistics (χ^2), the experimental data for kinetic study were accurately described by the Elovich model (R^2=0.975-0.980 and χ^2=0.212-0.304) than the pseudo-second-order (0.826-0.863 and 1.752-2.699) and pseudo-first-order (0.582-0.708 and 4.305-8.099) models, respectively. The better fit of experimental data with the Elovich model signified that the surfaces of the hydrochar samples are a non-homogenous system.

Additionally, the adsorption phenomenon occurred rapidly; approximately 55%, 44%, and 38% of the total MG5 in the solutions can be removed by GSH, CCH, and OPH within 1 minute, respectively. This observation is in line with the result of the initial adsorption rate (α; mg/g×min); the α values decreased in the order: GSH (5,743)>CCH (527)>OPH (131). The initial fast removal of GSH probably might result from its plentiful active sites (Table 1).

4. Adsorption Isotherms

Collecting adsorption isotherms is a useful strategy to both describe the relationship between the adsorbate concentration in the solution (liquid phase) and the adsorbent (solid phase) at a constant temperature and design adsorption systems. In this study, the Langmuir (Eq. (8)), Freundlich (Eq. (9)), and Dubinin-Radushkevich (Eqs. (10)-(12)) models were employed to describe the adsorptive behavior of cationic dye into the hydrochar. To minimize the respective error functions, the non-linear optimization technique was applied for calculating the parameters of these models.

$$q_e = \frac{Q^0_{max} K_L C_e}{1 + K_L C_e} \tag{8}$$

$$q_e = K_F C_e^n \tag{9}$$

$$q_e = q_{DR} e^{-K_{DR}\varepsilon^2} \tag{10}$$

$$\varepsilon = RT\ln\left(1 + \frac{1}{C_e}\right) \tag{11}$$

$$E = \frac{1}{\sqrt{2K_{DR}}} \tag{12}$$

where q_e and C_e are obtained from Eq. (1); Q^o_{max} (mg/g) is the maximum saturated monolayer adsorption capacity of adsorbent; K_L (L/mg) is the Langmuir constant related to the affinity between an adsorbent and adsorbate; K_F [(mg/g)/(mg/L)^n] is the Freundlich constant, which characterizes the strength of adsorption; n (dimensionless) is a Freundlich intensity parameter, which indicates the magnitude of the adsorption driving force or surface heterogeneity; the adsorption isotherm becomes linear with n=1, favorable with n<1, and unfavorable with n>1; q_{RD} (mg/g) is the adsorption capacity, K_{RD} (mol^2/kJ^2) is a constant related to the sorption energy, ε is the Polanyi potential, and E (kJ/mol) is the mean adsorption energy.

The complete adsorption isotherms of MG5 onto the hydrochars are illustrated in Fig. 6, and the corresponding adsorption parameters are in Table 3. Clearly, the adsorption of MG5 onto hydrochar can be adequately described using the Langmuir, Freundlich, and Dubinin-Radushkevich models because of high R^2 and low

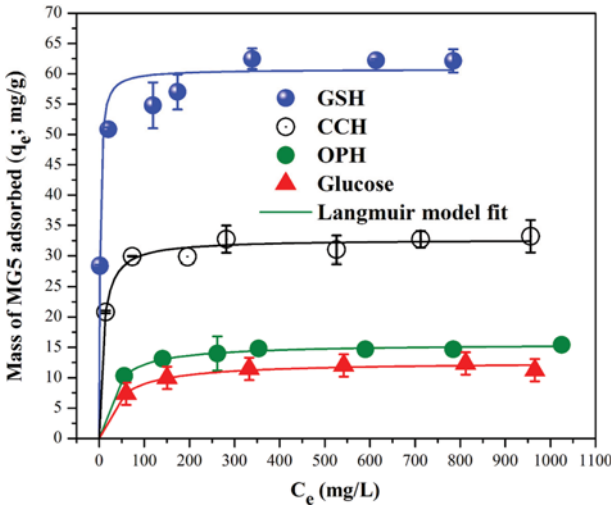

Fig. 6. Adsorption isotherms of MG5 adsorption onto three hydrochars and glucose samples (Experimental conditions: initial MG5 concentrations (approximately 100-1,100 mg/L), 0 M NaCl, contact time 24 h, temperature 30 °C, and initial solution pH 7.0).

χ^2 values. Furthermore, the monolayer adsorption capacities calculated from the Langmuir equation (Q^o_{max}) were nearly coincident with these from the Dubinin-Radushkevich equation (Q_{RD}). The maximum adsorption capacities of MG5 decreased with the selective order of GSH>CCH>OPH (Table 3), which agrees with the order of the surface charge density of acidic functional groups (Table 1) and adsorption energy (Table 3): GSH>CCH>OPH. In other words, the adsorption capacity of the hydrochar was directly proportional to the concentration of its surface acidic groups.

Moreover, the dye adsorption was greatly influenced by the operation temperatures. The amount of MG5 uptake decreased with increasing temperature. The Q^o_{max} values at 30 °C, 40 °C, and 50 °C were as follows: 59.6 mg/g>58.4 mg/g>56.9 mg/g for GSH (p<0.05), 32.7 mg/g>31.7 mg/g>30.7 mg/g for CCH (p<0.05), and 15.6 mg/g>14.8 mg/g>12.6 mg/g (p<0.05), respectively. The decreased adsorptive capacities at higher temperatures were caused by decreases in adsorption energies (Table 3).

The adsorption energy (E) values decreased from 1.067 to 0.091 kJ/mol for GSH, from 0.182 to 0.07 kJ/mol for CCH, and 0.052 to 0.032 kJ/mol for OPH when the reaction temperatures increased from 30 °C to 50 °C, respectively. In general, the low E magnitudes suggested the dye removal process involved in the physical adsorption. Particularly, the adsorption energies of MG5 onto hydrochars (0.032-1.067 kJ/mol) were similar to those of their precursors (biosorbents; 0.018-0.872 kJ/mol) reported in our previous study [26]. Thus, it would be expected that the adsorption mechanisms of MG5 onto hydrochars will be similar to biosorbents (i.e., electrostatic attraction, hydrogen bonding formations, and n-π interaction).

According to our previous results [9,25], at the same operation conditions, the maximum adsorption capacities of MG5 exhibited the following order: activated carbon>biosorbent>hydrochar>biochar. Taking golden shower as a typical example, the Q^o_{max} values of activated carbons prepared from various chemical activation methods ranged from 253 to 531 mg/g, and the Q^o_{max} value of commercial activated charcoal (Norit RB4C) was 489 mg/g. The Q^o_{max} value for biosorbent was approximately 106 mg/g, whereas the Q^o_{max} values for hydrochar and biochar were approximately 60 mg/g and 46 mg/g, respectively. The BET specific surface areas (m^2/g) and total pore volumes (cm^3/g) of golden shower adsorbents had the following other: activated carbons (812-1413 m^2/g and 0.38-0.68 cm^3/g)>biochar (598 m^2/g and 0.30 cm^3/g)>hydrochar> (14.7 m^2/g and 0.076 cm^3/g)>biosorbent (8.14 m^2/g and 0.011 cm^3/g). In contrast, the total acidic groups of golden shower adsorbents indicated the order: biosorbent (8.74 mmol/g)>hydrochar (2.12 mmol/g)>activated carbons (0.55-1.20 mmol/g)>biochar (0.72 mmol/g) [9,12,25]. Clearly, the maximum adsorption capacity of hydrochar toward MG5 was higher than biochar although its sur-

Table 3. Corresponding isotherm parameters for MG5 adsorption onto the hydrochar samples

	Langmuir parameters				Freundlich parameters				D-R parameters				
	Q^o_{max}	K_L	R^2	χ^2	K_F	n	R^2	χ^2	Q_{RD}	K_{RD}	R^2	χ^2	E
30 °C													
GSH	59.6	0.55	0.93	0.11	32.8	0.10	0.90	2.14	58.3	0.14	0.87	1.93	1.067
CCH	32.7	0.12	0.95	0.18	18.5	0.09	0.80	0.82	31.7	15.1	0.91	0.30	0.182
OPH	15.6	0.04	0.98	0.03	7.18	0.11	0.84	0.22	14.7	186	0.92	0.10	0.052
GH	12.6	0.02	0.94	0.09	4.60	0.14	0.79	0.14	11.7	281	0.91	0.12	0.042
40 °C													
GSH	58.4	0.05	0.99	0.12	22.5	0.15	0.81	3.59	53.8	28.9	0.88	1.82	0.132
CCH	31.7	0.07	0.99	0.03	14.7	0.12	0.88	0.58	30.3	31.9	0.91	0.36	0.125
OPH	14.8	0.03	0.84	0.46	4.98	0.15	0.76	0.99	16.8	402	0.97	0.07	0.035
50 °C													
GSH	56.9	0.03	0.98	0.50	14.3	0.21	0.88	3.77	50.9	61.0	0.89	3.09	0.091
CCH	30.7	0.04	0.89	0.62	12.5	0.13	0.78	1.94	29.0	102	0.96	0.21	0.070
OPH	12.6	0.02	0.93	0.17	3.48	0.18	0.79	0.54	11.5	467	0.98	0.05	0.032

Note: the units of isotherm parameters are Q^o_{max} (mg/g), K_L (L/mg), K_F (mg/g)/(mg/L)^n, n (dimensionless), Q_{RD} (mg/g), K_{RD} (mol^2/kJ^2), E (kJ/mol). The adsorption isotherms at 30 °C are shown in Figure 6, while the adsorption isotherms at 40 °C and 50 °C were not reported

face area was significantly lower, which resulted from different adsorption mechanisms between them.

As expected, the Q^o_{max} values of the synthesized hydrochars from agricultural wastes (GSH, CCH, and OPH) were higher than the Q^o_{max} of commercial glucose hydrochar (GH), suggesting that the synthesized hydrochars might be a potential candidate for removal cation dyes from aqueous media.

5. Adsorption Thermodynamics

Thermodynamic investigation plays an indispensable part in the prediction of adsorption mechanisms (e.g., physical or chemical). The thermodynamic parameters can be computed according to the thermodynamic laws through the following equations:

$$\Delta G^o = -RT\ln K_C \quad (13)$$

The relationship between ΔG^o and ΔH^o and ΔS^o is described as follows:

$$\Delta G^o = \Delta H^o - T\Delta S^o \quad (14)$$

The well-known van't Hoff equation is obtained by substituting Eq. (14) into Eq. (13)

$$\ln K_C = \frac{-\Delta H^o}{R} x \frac{1}{T} + \frac{\Delta S^o}{R} \quad (15)$$

where R is a universal gas constant (8.3144 J/mol×K), and T is absolute temperature in Kelvin (K=273+°C).

The Gibbs energy change (ΔG^o) is directly calculated from Eq. (13), while the enthalpy change (ΔH^o) and the entropy change (ΔS^o) are determined from the slope and intercept, respectively, of a plot of $\ln K_C$ against 1/T (Eq. (15)). It is well-known that the equilibrium constant (K_C) must be dimensionless. In this study, the K_C derived from the Langmuir constant (K_L) was used for calculation of the thermodynamic parameters—ΔG^o, ΔH^o, and ΔS^o because the adsorption equilibrium data were accurately described by the Langmuir model (see Fig. 6). The K_C can be easily obtained as a dimensionless parameter by multiplying K_L by 433 g/mol (MG5 molecular weight), 1,000, and then 55.5 (the number of moles of pure water per liter) [9,26].

The profiles of thermodynamic parameters are listed in Table 4. The equilibrium constants (K_C) decreased dramatically when the solution temperatures increased, which confirms that the adsorption process was favorable at a lower temperature and exothermic. This conclusion matches well with the results obtained from the adsorption isotherms; the maximum monolayer adsorption capacity indicated a decreasing tendency at a higher temperature.

In addition, the ΔG^o exhibits a negative quantity, demonstrating that the adsorptive process occurred favorably and spontaneously with low adsorption-energy requirements at a given temperature. This result accords with the hypothesis of the exponent n of the Freundlich equation in Section 4.

The negative ΔH^o values suggested the exothermicity of the adsorption process, which was demonstrated by a decrease in the maximum adsorption capacity (Q^o_{max}) and the equilibrium constant (K_C) with higher-temperature conditions. The exothermicity might also imply the emission of energy in form of heat into its surroundings during the adsorptive process.

Notably, ΔS^o exhibits the opposite trend relative to those of ΔH^o and ΔG^o for the three hydrochars. The dye adsorption phenomenon onto the GSH and CCH samples becomes less random ($\Delta S^o < 0$), while that onto OP was increasingly random ($\Delta S^o > 0$). This difference involves the sign of the entropy change and may indicate that these materials exhibit different adsorption mechanisms. The difference will be thoroughly discussed in the desorption study (Section 6) and adsorptive mechanism analysis (Section 7).

6. Desorption Study

Studying the desorption of cationic dyes can be used to gain insights into their adsorption characteristics. Fig. 7 presents percentage of desorption of MG5 by using various desorption agents, such as deionized distilled water at pH 2, hydrochloric acid, sodium chloride, and methanol. If the adsorption mechanism only involved electrostatic attraction between the negatively charged groups (i.e., $-COO^-$) on the hydrochar's surface and MG5 cationic molecules, the adsorption should be completely desorbed in the H^+ aqueous environment. However, the percentage of MG5 desorbed by deionized distilled water pH 2 and HCl (0.1 M) was approximately 49-79% and 59-77%, respectively, suggesting that there is the presence of other interactions in adsorption mechanisms. Assumption on the percentage of MG5 desorbed by methanol corresponded with the interactions of oxygen functional groups (i.e., hydrogen bond-

Table 4. Thermodynamic parameters for MG5 adsorption process onto the hydochar samples

T (K)	Van't Hoff equation	K_C	ΔG^o (kJ/mol)	ΔH^o (kJ/mol)	ΔS^o (J/mol×T)
Golden shower pod hydrochar (GSH)					
303	y=1,4448x−32 R^2=0.898	13,294,226	−41.34	−120	−262
313		1,240,025	−36.53		
323		708,929	−36.20		
Coconut shell hydrochar (CCH)					
303	y=5608x−3.61 R^2=0.999	2,934,246	−37.52	−46.6	−30.1
313		1,658,174	−37.27		
323		932,422	−36.91		
Orange peel hydrochar (OPH)					
303	y=3878x+0.83 R^2=0.964	862,731	−34.43	−32.2	6.88
313		502,258	−34.16		
323		391,713	−34.59		

ing and n-π interaction), it can be concluded that these interactions contributed approximately 19-30%.

Our recent investigation results [9,12,25] demonstrated that the adsorption process of MG5 onto the biochar, synthesized activated carbons, and commercial activated carbon was irreversible because of the dominant contribution of π-π interaction than others (i.e., pore filling, hydrogen bonding, and n-π interaction). However, the adsorption process of MG5 onto biosorbent was reversible because the primary mechanisms are electrostatic interactions (>16% for GS, 28% for CC, and >60% for OP) and other interactions (i.e., hydrogen bonding and n-π interaction; approximately 76% for GS, 62% for CC, and 34% for OP).

7. Adsorption Mechanism Analysis

7-1. Pore Filling Formation

The hydrochar samples exhibit low BET surface areas (6.65-14.7 m^2/g) and total pore volumes (0.0025-0.076 cm^3/g); therefore, the contribution of pore filling in adsorption mechanisms is negligible. The other contributions (electrostatic attraction, hydrogen bonding formation, n-π interaction, and π-π interaction) might play an important role in the adsorbent-adsorbate interactions.

As shown in our recent studies [8,9], the specific surface areas, non-micropore volumes, and total pore volumes of the carbonaceous porous materials (prepared biochar, synthesized activated carbons, and commercial activated carbon) simultaneously decreased after MG5 adsorptions, suggesting that pore filling has a certain contribution to the MG5 adsorption mechanism. Particularly, at low initial MG5 concentration (approximately 50 mg/L) with approximately 99% removal rate, the S_{BET} (m^2/g) and total pore volume (cm^3/g) of orange peel-prepared biochar (OPB) before adsorption (565 m^2/g and 0.2356 cm^3/g) are similar to OPB after adsorption (529 m^2/g and 0.2635 cm^3/g). However, at higher MG5 concentration (approximately 340 mg/L), there is a remarkable decrease regarding S_{BET} and V_{total} of MG5-laden OPB to 13.5 m^2/g and 0.023 cm^3/g, respectively. On the basis of analysis and discussion regarding the intra-particle model and BET surface area, we proposed that (1) there is co-existence of other interactions than pore filling in MG5 sorption mechanisms and (2) the contribution of pore filling at low initial dye concentrations is negligible.

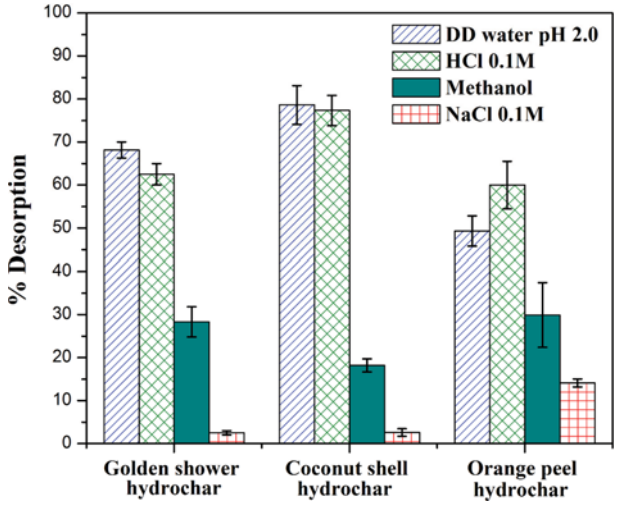

Fig. 7. Percentage of MG5 desorbed using different desorbing agents.

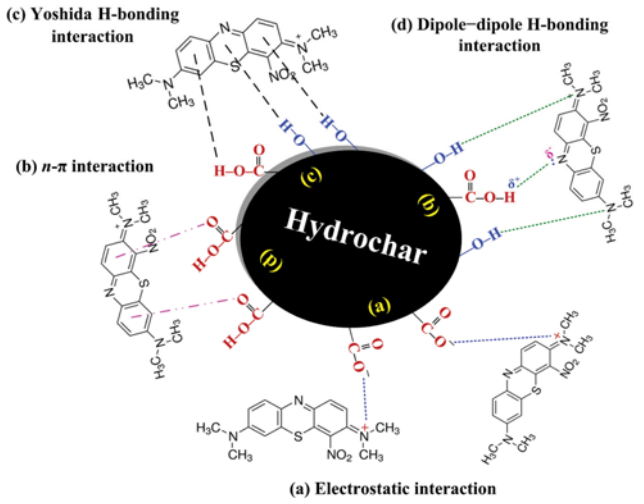

Fig. 8. Proposed adsorption mechanisms of MG5 onto the hydrochar samples.

7-2. Electrostatic Attraction

This mechanism can be discussed according to the experimental condition that was conducted at the pH of initial MG5 solution, approximately 7.0. Clearly, at this pH level, the electrostatic attractions played a major role in the adsorption mechanisms (Fig. 8(a)), which can be confirmed by the analysis of pH values after adsorption (Fig. 4(d)) and desorption study (Fig. 7). The decreasing degree of pH after adsorption ($-\Delta pH=pH_{after}-pH_{initial}$) followed CCH (2.265-3.125)>GSH (1.765-2.715)>OPH (0.435-2.01). This order was dissimilar to the order of the carboxylic groups on the hydrochar's surface (Table 1): GSH (0.76 mmol/g)>CCH (0.67 mmol/g)>OPH (0.41 mmol/g), indicating the presence of other mechanisms in GSH.

7-3. n-π Interactions

The n-π interaction was originally proposed by Mattson and colleagues [27], who investigated the adsorption phenomenon of phenol and nitro-phenols onto activated carbon. The comparison results of FTIR before and after adsorption (Fig. 3) showed that the C=O peaks of GSH decreased its intensity and shifted to lower wavenumber from 1,697 to 1,689 cm^{-1}, confirming the presence of n-π interactions (known as n-π electron donor-acceptor interactions) [8,9,25,27-29]. In contrast, the CCH and OPH samples demonstrated the insignificant change of the C=O peak positions after adsorption from 1,695 to 1,696 cm^{-1} and from 1,695 to 1,697 cm^{-1}, respectively. Therefore, it can be concluded that the carboxylic groups on the surface of GSH sample were responsible for both the electrostatic attractions (Fig. 8(a)) and n-π interactions (Fig. 8(b)).

7-4. Hydrogen Bonding Formation

The π-π interaction (also known as π-π electron donor-acceptor interactions) was initially proposed by Coughlin and Ezra [30] who studied the role of acidity groups on the surface of carbon in adsorbing organic pollutants in aqueous solutions. Fig. 3 proves that the peaks corresponding to -OH groups decreased and shifted slightly after adsorption, from 3,360 to 3,353 cm^{-1} for GSH, 3,356

to 3,351 cm^{-1} to CCH, and 3,353 to 3,350 cm^{-1} for OPH. This result suggested that the hydrogen bonding can occur neither (1) between surface hydrogen bonds on the hydrochar's surface and the aromatic rings in MG5 structure, nor (2) between surface hydrogen bonds of the hydroxyl groups (H-donor) on the hydrochar's surface and the atoms (i.e., nitrogen and oxygen; H-acceptor). The former was known as the Yoshida H-bonding (Fig. 8(c)), and the latter was known as the dipole-dipole H-bonding (Fig. 8(b)) [8,9,25,29,31,32].

7-5. π-π Interactions

Fig. 1 shows that every MG5 molecule has a polar nitro functional group (electron-withdrawing) on the benzene ring. Nitrogen groups often act as strong electron acceptors [29]; therefore, the presence of aromatic carbon structures (C=C) in the hydrochar samples was expected as π-π interactions occurring between π-electron in the carbon and the π-electron in the aromatic ring of MG5 molecules.

Generally, the addition of oxygen- and nitrogen-containing functional groups (electron-withdrawing) at the edges of the individual graphene layers within carbonaceous materials (i.e., biochar, activated carbon, and graphene) causes a considerable drop in the π-electron density of the carbonaceous materials. Positive holes are consequently created in the conduction π-band of the individual graphene layers, and the interactions between the π-electrons of the carbonaceous materials and aromatic pollutants (i.e., phenol and dye) become weaker [9,29,30].

Recently, Huff and Lee [33] investigated the surface oxygenation of pinewood-derived biochar using H_2O_2 and found that methylene blue adsorption onto the biochar decreased when higher H_2O_2 concentrations were used in the treatment. They emphasized that the addition of oxygen groups onto the aromatic ring structure of the biochar weakened the π-π interactions that were mainly responsible for adsorption of the dye onto the untreated biochar surface. Additionally, Demir-Cakan and coworker [34] prepared the carboxylate-rich carbonaceous material (also known as hydrochar) through a one-step hydrothermal carbonization of glucose. Noticeably, in our recent studies [8,9], we synthesized the carbonaceous materials (golden shower-derived biochar and activated carbons, and commercial activated carbon) with the abundant oxygen-containing functionalities on their surface through a new process of the two-step carbonizations. This method could be an effective approach for preparing oxygen-functional-group-rich carbonaceous materials without significantly affecting their textural properties. It was concluded that oxygenation of the surface of the carbonaceous materials through a hydrothermal process with acrylic acid resulted in a decrease in MG5 adsorption and identified the importance of π-π interactions to the adsorption process.

In this study, we used two pieces of experimental evidence to consider whether there is the existence of π-π interactions between the π-electrons of hydrochar and the π-electrons of the aromatic rings of MG5.

First, the addition of oxygen groups to aromatic ring structure of hydrochar contributed to significantly increase the adsorption of MG5 (Fig. 9), which is confirmation of the negligible roles of π-π interactions [9,33]. This is because hydrochar was prepared through the hydrothermal process with a low carbonization degree (190 °C, 4 h). As mentioned in Section Introduction, the degree of aromatization and carbonization can be described by neither the H/C molar ratio (using element analyzer) nor onset and endset temperatures (using thermo-gravimetric analysis). Our investigation [12] reported that the relatively higher H/C molar ratio of GSH (0.62) indicates that original organic plant residues, such as cellulose and lignin remained in hydrochar. The H/C ratios of golden shower-derived biosorbent (GS) and biochar (GSB) are 0.56 and 0.20, while golden shower-activated carbons prepared from various chemical activated methods with K_2CO_3 (GSAC, GSBAC, GSHAC) possess low H/C ratios (0.10, 0.03, and 0.06), respectively. Meanwhile, the onset and endset temperatures followed the synthesized activated carbons (553-476 °C and 683-695 °C)>GS biochar (414 °C and 579 °C)>GS hydrochar (286 °C and 544 °C)>GS biosorbent (246 °C and 489 °C), respectively. It can be concluded that hydrochar exhibited a low level of aromatization and carbonization (weak C=C aromatic carbon structures); therefore, the presence of π-π interactions in adsorption mechanism seems negligible.

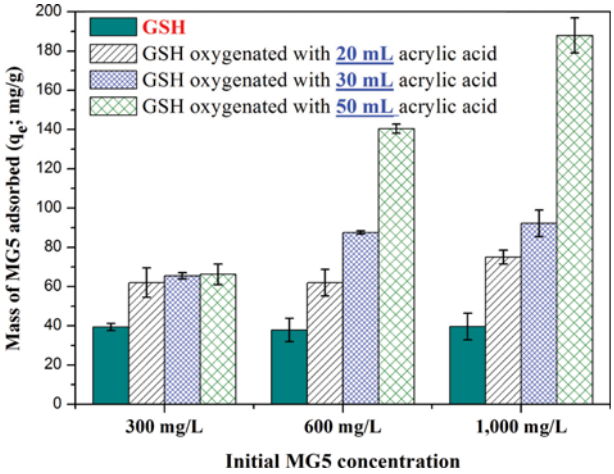

Fig. 9. Comparison of the adsorption capacities of the non-oxygenated hydrochars and the oxygenated hydrochars (Experimental conditions: 30 °C, 0 M NaCl, contact time 24 h, and initial solution pH 7.0).

Furthermore, because of the negligible contributions of π-π interaction, the amount of MG adsorbed on hydrochar will be directly proportional to the added amount of oxygen-containing acidic functional groups (Fig. 9). Assumption is that the added amount of oxygen functionalities is be directly proportional to the used volume of acrylic acid. This result is in good accordance with our recent study [14]. In [14], we synthesized glucose-derived carbon sphere functionalized with Triethylenetetramine (spherical hydrochar functionalized with TETA) and applied it for the removal of acid red 1, MG5, and phenol from aqueous solutions. The adsorption results revealed that the maximum adsorption capacities of the spherical hydrochar functionalized with TETA (Q^o_{max}=36.1 mg/g for AR1, 67.6 mg/g for MG, and 137 mg/g for phenol) were significantly higher than those of the spherical hydrochar without TETA (Q^o_{max}=21.2 mg/g, 11.4 mg/g, 13.9 mg/g, and 11.4 mg/g), respectively. Therefore, it can be concluded that the addition of oxygen- and nitrogen-containing functional groups (the electron-with-

drawing groups) on the surface of hydrochar did not cause a considerable drop in the π-electron density, but the oxygenation and functionalization processes provided abundant adsorption sites on the hydrochar's surface.

Second, FTIR analysis demonstrated that the peaks corresponding to the aromatic C=C bonds did not indicate a decrease in intensity and a shift of their wavenumber positions after adsorption of MG5 (Fig 3). The result of FTIR analysis is different from the results obtained by other scholars [8,9,29,35]. For example, Xu and coworkers [35] studied the adsorption phenomenon of bisphenol A in an aqueous solution onto graphene. They concluded that π-π interactions existed between the benzene rings of bisphenol A and graphene planes after observing an upshift of the graphene C=C bond peak from 1,633 to 1,641 cm^{-1} upon bisphenol A adsorption on graphene. In addition, they concluded that compared to other carbonaceous materials (biochar and activated carbon), graphene has larger and smoother surfaces for forming π-π interactions that can easily adsorb more organic contaminants. Similarly, Tran and colleagues [8] pointed out that the peak corresponding to the skeletal vibration of aromatic C=C bonds in commercial activated carbon decreased in intensity and upshifted after MG5 adsorption (1,537 cm^{-1} to 1,561 cm^{-1}). This upshift indicates the presence of π-π interactions between commercial activated carbon and MG5. Therefore, the π-π electron donor-acceptor interactions were not dominantly responsible for the adsorption of MG5 onto the hydrochar.

The primary adsorption mechanisms of MG5 by the hydrochars are summarized in Fig. 8. The concentrations of total acid groups (i.e. carboxylic and phenolic) on the hydrochar's surface determined the selective adsorption order of the adsorbents: GSH>CCH> OPH.

CONCLUSIONS

Agricultural wastes-derived hydrochars prepared through hydrothermal carbonization process exhibited low porosities with low specific (BET) surface areas (6.65-014.7 m^2/g) and total pore volumes (0.0024-0.076 cm^3/g), but abundant oxygen functional active groups (1.69-2.12 mmol/g). The density of carbon spheres was strongly dependent on the HTC conditions. The optimal condition of HTC using 0 M NaOH was at 190 °C for 24 h.

The dye removal process was greatly affected by the pH solution and the presence of Na^+ and Cl^- ions. The kinetic study suggested that adsorption can reach fast equilibrium in approximately 60-120 min, and a removal rate of 38-55% can be generated within 1 min. The maximum adsorption capacities at 30 °C were ranked as follows: GSH (59.6 mg/g)>CCH (32.7 mg/g)>OPH (15.6 mg/g)>GH (12.6 mg/g). The thermodynamic investigation demonstrated that the adsorption process was spontaneous ($-\Delta G^o$) and exothermic ($-\Delta H^o$).

Unlike biochar and activated carbon, hydrochar has weaker aromatic ring structure; therefore, its adsorption capacity for a cationic dye can be enhanced when its surface was oxygenated because of the absence of π-π interaction.

The PZC of the hydrochar was useful to explain the effects of solution pH on adsorption capacity. Similarly, the concentrations of oxygen acidic functional groups on the hydrochar's surface determined the selective order of hydrochars. The dominant adsorption mechanisms were electrostatic attraction, while hydrogen bonding and n-π interactions played minor roles. The adsorption mechanisms of MG5 onto hydrochar were similar to biosorbent, but dissimilar to other carbonaceous materials (i.e., biochar and activated carbon).

At the same operation conditions, the maximum MG5 adsorption capacities of golden shower material exhibited the following order: activated carbons (Q^o_{max}; 253-531 mg/g)>biosorbent>(106 mg/g)> hydrochar (60 mg/g)>biochar (46 mg/g). The Q^o_{max} values of commercial activated charcoal and commercial glucose hydrochar were 489 mg/g and 12.6 mg/g, respectively.

ACKNOWLEDGEMENTS

This current work was financially supported by Chung Yuan Christian University (CYCU) in Taiwan. The first author would like to thank CYCU for the Distinguished International Graduate Students (DIGS) scholarship to pursue his doctoral studies.

REFERENCES

1. F. M. D. Chequer, G. A. R. de Oliveira, E. R. A. Ferraz, J. C. Cardoso, M. V. B. Zanoni and D. P. de Oliveira, *Eco-friendly Textile Dyeing and Finishing*, INTECH Publishers, 151 (2013).
2. N. P. Raval, P. U. Shah and N. K. Shah, *Environ. Sci. Pollut. r.*, **23**, 14810 (2016).
3. G. Crini, *Bioresour. Technol.*, **97**, 1061 (2006).
4. E. Contreras, L. Sepúlveda and C. Palma, *Int. J. Chem. Eng.*, **2012**, 1 (2012).
5. N. Feng, X. Guo and S. Liang, *J. Hazard. Mater.*, **164**, 1286 (2009).
6. H. N. Tran, S.-J. You and H.-P. Chao, *Waste Manage. Res.*, **34**, 129 (2016).
7. J. S. Cha, S. H. Park, S. C. Jung, C. Ryu, J. K. Jeon, M. C. Shin and Y. K. Park, *J. Ind. Eng. Chem.*, **40**, 1 (2016).
8. H. N. Tran, Y.-F. Wang, S.-J. You and H.-P. Chao, *Trans. IChemE Process Saf. Environ. Prot.*, (2017), DOI:10.1016/j.psep.2017.02.010.
9. H. N. Tran, S.-J. You and H.-P. Chao, *J. Environ. Manage.*, **188**, 322 (2017).
10. J. A. Libra, K. S. Ro, C. Kammann, A. Funke, N. D. Berge, Y. Neubauer, M. M. Titirici, C. Fühner, O. Bens, J. Kern and K. H. Emmerich, *Biofuels*, **2**, 71 (2011).
11. A. Jain, R. Balasubramanian and M. P. Srinivasan, *Chem. Eng. J.*, **283**, 789 (2016).
12. H. N. Tran, S.-J. You and H.-P. Chao, *Adsorpt. Sci. Technol.*, (2017), DOI:10.1177/0263617416684837.
13. A. Funke and F. Ziegler, *Biofuel. Bioprod. Bior.*, **4**, 160 (2010).
14. H. N. Tran, F.-C. Huang, C.-K. Lee and H.-P. Chao, *Green Process. Synth.*, (2017), DOI:10.1515/gps-2016-0178.
15. S. L. Goertzen, K. D. Thériault, A. M. Oickle, A. C. Tarasuk and H. A. Andreas, *Carbon*, **48**, 1252 (2010).
16. M. Sevilla and A. B. Fuertes, *Chem. Eur. J.*, **15**, 4195 (2009).
17. M. Sevilla and A. B. Fuertes, *Carbon*, **47**, 2281 (2009).
18. M. Sevilla, J. A. Maciá-Agulló and A. B. Fuertes, *Biomass Bioenergy*, **35**, 3152 (2011).

19. M. Sevilla, A. B. Fuertes and R. Mokaya, *Energy Environ. Sci.*, **4**, 1400 (2011).
20. M. Doğan, H. Abak and M. Alkan, *J. Hazard. Mater.*, **164**, 172 (2009).
21. Y. Guo, S. Yang, W. Fu, J. Qi, R. Li, Z. Wang and H. Xu, *Dyes Pigments*, **56**, 219 (2003).
22. S. Lagergren, *Ksver. Veterskapsakad. Handl.*, **24**, 1 (1898).
23. G. Blanchard, M. Maunaye and G. Martin, *Water Res.*, **18**, 1501 (1984).
24. S. H. Chien and W. R. Clayton, *Soil Sci. Soc. Am. J.*, **44**, 265 (1980).
25. H. N. Tran, S.-J. You and H.-P. Chao, *Chem. Eng. Commun.*, (2017), DOI:10.1016/j.watres.2017.04.014.
26. H. N. Tran, S.-J. You and H.-P. Chao, *J. Environ. Chem. Eng.*, **4**, 2671 (2016).
27. J. A. Mattson, H. B. Mark, M. D. Malbin, W. J. Weber and J. C. Crittenden, *J. Colloid Interface Sci.*, **31**, 116 (1969).
28. B. Xing, W. B. McGill, M. J. Dudas, Y. Maham and L. Hepler, *Environ. Sci. Technol.*, **28**, 466 (1994).
29. L. R. Radovic, C. Moreno-Castilla and J. Rivera-Utrilla, *Chemistry and physics of carbon*, Marcel Dekker, Inc., New York, **27**, 227 (2000).
30. R. W. Coughlin and F. S. Ezra, *Environ. Sci. Technol.*, **2**, 291 (1968).
31. R. S. Blackburn, *Environ. Sci. Technol.*, **38**, 4905 (2004).
32. M. A. Al-Ghouti, M. A. M. Khraisheh, S. J. Allen and M. N. Ahmad, *J. Environ. Manage.*, **69**, 229 (2003).
33. M. D. Huff and J. W. Lee, *J. Environ. Manage.*, **165**, 17 (2016).
34. R. Demir-Cakan, N. Baccile, M. Antonietti and M. M. Titirici, *Chem. Mater.*, **21**, 484 (2009).
35. J. Xu, L. Wang and Y. Zhu, *Langmuir*, **28**, 8418 (2012).